Applications of Observational Radio Astrophysics

K. Schutz*
MIT Department of Physics
(Dated: November 6, 2012)

Using a small radio telescope (SRT) on the roof of Building 26, we explored various applications of observational radio astrophysics. We measured the brightness temperature of the sun to determine levels of solar activity. Additionally, we took advantage of 21 cm hyperfine splitting of neutral hydrogen as well as the Doppler shift relation to obtain a galactic rotation curve for the Milky Way. If we compare our experimentally derived rotation curve to the predictions of Keplerian orbital mechanics, we find that ordinary luminous matter cannot account for the velocities for galactic radii greater than 3 kpc. These observations are consistent with the rest of the evidence for dark matter. We also used our rotation curve to determine Oort's constants A and B, as well as to map the Norma, Orion-Cygnus, Saggitarius-Carina, and Perseus spiral arms of the milky way.

I. INTRODUCTION

21 cm radiation is a remarkably powerful tool in observational astrophysics. Due to their relatively long wavelengths, 21 cm radio waves rarely scatter off of material in the foreground, such as galactic dust or the atmosphere. Thus 21 cm signals are far less attenuated than those of visible frequencies. We can use these radio waves to observe parts of black body spectra from objects such as the sun. We can also use a narrow frequency band around 1420.4 MHz to detect the 21 cm signal from hyperfine flip transitions of neutral hydrogen. This small change in atomic energies is the result of the spin interactions of the proton and electron. Any shift from 1420.4 MHz is indicative of Doppler effects from the hydrogen moving relative to the observer.

II. BACKGROUND THEORY

II.1. Brightness Temperature of the Sun

The brightness temperature of an object is the temperature of a perfect blackbody (of the same angular size as the object) that produces the observed intensity of that object in a given frequency band. We measure intensity in terms of antenna temperature, the power per frequency bandwidth divided by Boltzmann's constant. Thus, the brightness temperature of the sun is given by the following equation:

$$T_{sun} = 2T_{antenna}\frac{\Omega_{HPBW}}{\Omega_s}. \quad (1)$$

The factor of 2 accounts for the fact that the antenna only picks up one polarization of light, whereas light from the sun is unpolarized. Ω_{HPBW} is the half-power beam width of the antenna (which in our case follows an Airy diffraction pattern) and Ω_s is the solid angle of the sun [3].

The sun radiates like a blackbody with a temperature of 6000 K with varying behavior at radio frequencies depending on sunspots and other solar activity. Its brightness temperature at wavelengths near 21 cm is between $10^5 - 10^6$ K, depending on whether one observes the chromosphere or corona, and depending on whether we are in a quiet sun part of the solar cycle [3]. We can use experimentally determined solar brightness temperatures as a metric of the level of current solar activity.

II.2. The Structure of the Milky Way

Our galaxy, the Milky Way, is comprised of two parts. In the center, there is a dense spheroid bulge with a radius of approximately 3 kpc. It is surrounded by a thin disk of thickness 200 pc with a radius extending out to approximately 30 kpc [1]. The disk has a spiral arm structure whose origin and mechanism are an open area of research. One popular theory, Lin-Shu density wave theory, says that the arms are like envelopes of a density wave packet. However poorly we may understand the structure, we know that our sun is located in the Orion-Cygnus arm, at approximately 8 kpc from the galactic center [1].

II.3. The Dynamics of the Milky Way

Despite the rareness of the hyperfine flip transition, we expect to see a strong signal at around 1420.4 MHz from the neutral hydrogen in our galaxy, since it is incredibly abundant in the interstellar medium. We can observe how quickly galactic hydrogen is moving relative to us in the line-of-sight direction by using the Doppler shift.

The disk structure of the outer part of the Milky Way intuitively suggests that the whole thing is rotating. Our sun rotates about the galactic center with a velocity of approximately 225 km/s [1]. We expect, given the structure of the Milky Way and our knowledge of Keplerian orbital dynamics, that the thin galactic disk will rotate about the dense central bulge approximately like $v \sim 1/\sqrt{r}$, which is the rotational velocity of an object in a circular orbit about a central mass.

* kschutz14@mit.edu

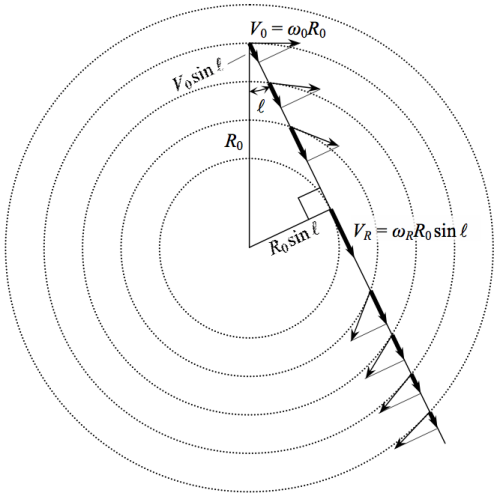

FIG. 1. In order to determine a rotation curve, it is imperative to have a way of knowing both where objects are spatially and how quickly they are rotating. We can see from this diagram that in order to fully satisfy the first condition, we must use the tangent point of the circular orbit of the object, which has radius of $R_0 \sin(l)$, because that uniquely corresponds to the point with the greatest recessional velocity relative to the observer [2]. We can then use geometry to determine its rotational velocity.

We can determine how quickly other things are rotating by using the Doppler shift as well as a bit of clever geometry [2], illustrated in Figure 1. By taking both of these into consideration, as well as knowledge about how fast we are moving relative to our local standard of rest (LSR) in the direction of viewing, we determine the rotation velocity to be the following:

$$V_r = \frac{\nu_0 - \nu}{\nu_0} c - V_{LSR} + V_0 \sin(l). \tag{2}$$

The first term accounts for the Doppler shift, where we consider ν_0 to be 1420.4 MHz and the waves' velocity, c, to be the speed of light in a vacuum. The second term, V_{LSR}, accounts for earth's velocity relative to the LSR in the direction of the line of sight. The final term accounts for the geometry at which we are viewing the rotation, where we consider the rotational velocity of the observers, V_0, to be 225 km/s and where l is the galactic longitude.

By determining how other parts of the galaxy rotate, we can calculate Oort's constants A and B [6], which are given below:

$$A = \frac{1}{2}\left(\frac{V_0}{R_0} - \frac{dV}{dR}\Big|_{R_0}\right) \tag{3}$$

$$B = -\frac{1}{2}\left(\frac{V_0}{R_0} + \frac{dV}{dR}\Big|_{R_0}\right). \tag{4}$$

Oort's constants determine orbital properties of the sun as well as local (around $R_0 = 8.33 \pm 0.35$ kpc) properties of the galactic disk, such as the mass density. We can also use them to extrapolate information about galactic rotation to galactic radii greater than that of the sun. For example, one can easily derive Oort's constant A to be $3V_0/4R$ for our Keplerian prediction, whereas we find that it is $V/2R_0$ for a rotation curve that is flat.

Finally, we can map hydrogen dense regions using our extrapolated knowledge of the rotational properties of the galaxy at various radii. Following Mihalas and Binney [2], the radii and polar angles of these dense regions are given by:

$$R = \frac{R_0 V \sin(l)}{V_r + V_0 \sin(l) + V_{LSR}} \tag{5}$$

$$\phi = \pi/2 - l + \arccos\left(\frac{R_0 sin(l)}{R}\right). \tag{6}$$

III. THE EXPERIMENT

III.1. SRT Signal Chain

We measured power spectra using an SRT consisting of a parabolic dish antenna with diameter of 7.5 feet and with a half-power beam width of approximately 7°. The signal was focused into the antenna feedhorn and passed through a low noise amplifier and a 40 MHz bandpass filter. Finally the signal is sent through the mixer that sets the center frequency of the output to that of the local oscillator (LO) by means of clever trigonometry [4].

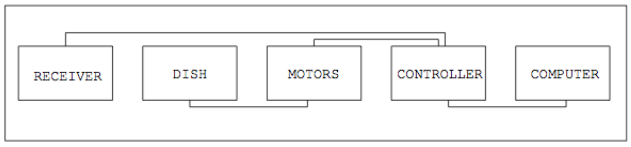

FIG. 2. A very basic block diagram of the SRT apparatus, taken from the labguide: http://web.mit.edu/8.13/www/JLExperiments/JLExp46.pdf

III.2. Methods and Procedures

We operated the telescope via the Junior Lab SRT software, which sets the LO frequency, number of frequency bins, bin width, and number of roll-off channels. It also controls the orientation of the antenna by means of a micro controller. The software allowed us to point the telescope at relevant points on the sky, such as the sun and various galactic coordinates. It also continually tracked the corresponding astrophysical objects (based on local sidereal time) and repositioned the antenna accordingly so the objects were constantly in the field of view.

We also used the software to calibrate the system by pointing the antenna at a test point corresponding to an empty point on the sky and by activating a noise diode with the approximate intensity and spectral distribution of a 115 Kelvin blackbody [4].

We took six offset scans of the sun to determine the beam pattern. We took data at angular offsets between -30° and 30° spaced at 1° increments in both the azimuthal and elevation directions. We also took several 5×5 scans to determine how accurate the software's tracking was, and whether there was any discrepancy between where the antenna was physically pointing and where the software indicated it was pointing.

We measured the power spectra at galactic longitudes between 5° and 250°, which is all of the galactic plane that is visible in the northern hemisphere in October. We integrated the spectra for approximately half an hour to increase our signal-to-noise ratio. We took data at each galactic longitude with 156 frequency bands spaced by 7.81 kHz. We took two datasets for each galactic longitude: one with the LO set to 1420.4 MHz and the other with the LO set to 1419.6 MHz. We did this in order to establish maximum velocity cutoffs that corresponded to frequencies outside of the first frequency band. We also used the software to determine our velocity relative to the local standard of rest, V_{LSR}, in the direction of our line of sight. This was crucial in accurately determining relative velocity between the galactic solar neighborhood and other parts of the galaxy.

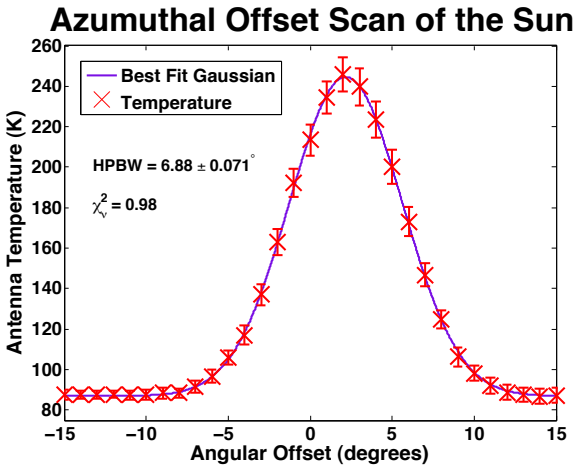

FIG. 3. 6 reduced azimuthal scans of the sun between offsets of -15° and 15° at 1420.4 MHz. The errors were the standard deviation of temperature at each offset divided by $\sqrt{n}$. We fit a Gaussian to this data and determined the maximum relative antenna temperature to be 156.62 ± 1.99 Kelvin. We took the difference between the center of the peak and 2σ and find the HPBW to be 6.88 ± 0.071°.

IV. DATA AND ANALYSIS

IV.1. Solar Brightness Temperature

We fit six azimuth and elevation offset scans to a Gaussian to find the half-power beam width (HPBW) and antenna temperature. The azimuthal offset scans are more reliable because there were buildings in our path during elevation scans. We have included the azimuth scans in Figure 3.

We took the half-power beam width to be 2σ and the antenna temperature to be the maximum temperature. We found the HPBW to be 6.88 ± 0.071°. Using Equation 1 along with standard propagation of errors techniques, we found the brightness temperature of the sun to be (1.96 ± 0.15) × 10^5 K.

IV.2. Milky Way Rotation Curve

The first and last ten frequency bins are unreliable because the receiver gain rolls off. We disregard those frequency bins for our analysis of the hydrogen power spectra.

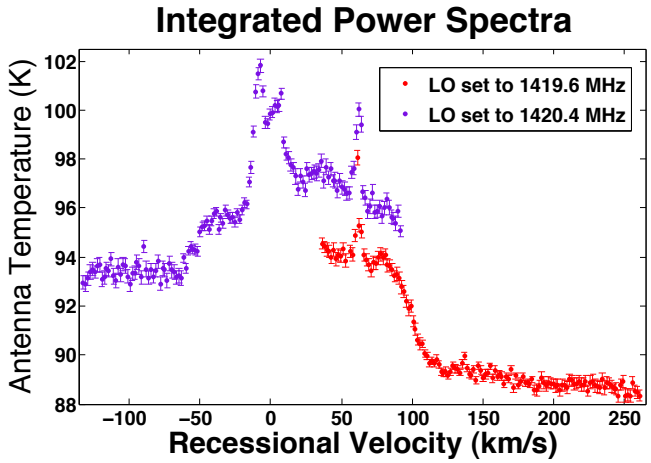

FIG. 4. These are an example of integrated power spectra at 25° galactic longitude. We took the errors to be the standard deviation of temperature in each frequency bin divided by $\sqrt{n}$. The error bars are relatively small due to the fact that we integrated our data for so long. These spectra have different vertical offsets because they were taken at different times, and thus have different background noise levels. However, we can see that the overall structure is maintained in the overlapping sections. Moreover, we are not interested in the temperature, but rather are interested in the point where the interesting spectral features hit the noise floor so that we can determine maximum recessional velocity.

We integrated our galactic power spectra for approximately half an hour per frequency band. An integrated power spectrum at a galactic longitude of 25° is shown in Figure 4. We used these power spectra to determine the maximum recessional velocities, which allow us to make use of the tangent-point geometry we previously discussed. We used the method of van de Hulst [5] and fit a linear regression to both the noise floor and the linear part of the relevant hydrogen features, and using these best-fit lines, we determined their intersection to be the maximum.

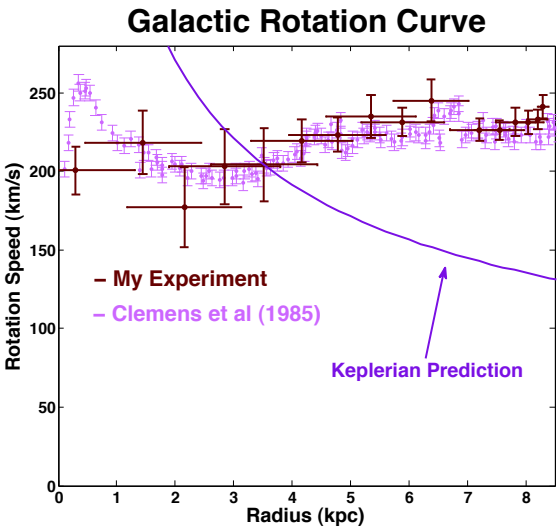

FIG. 5. We used Equation 2 to determine our rotation curve, which we overlay with the widely accepted rotation curve from Clemens et al. [8]. Despite the low angular resolution of our instrument and our time constraints, we see excellent agreement with their rotation curve. Our vertical error bars are determined by both statistical and systematic error, including our knowledge of the nontrivial 7° beam width, plus a 5% systematic error. In addition, we incorporated our knowledge of the expanding 3-kpc arm [2] and added an additional error of 7km/s for radii between 2 and 4 kpc. The horizontal error bars are determined by the 7° beam width. We also fit a Keplerian $1/\sqrt{r}$ curve based on the assumption that the galaxy is dense until 3kpc and then thins out in the disk [1]. Even if we fit this curve to the velocity at 3 kpc plus 1σ, we can see that the data are clearly not in agreement with this hypothesis.

Statistical uncertainties in the best fit lines were propagated through to the determination of the maximum velocity. In addition to these statistical uncertainties, we conservatively estimate 5% additional systematic uncertainty to account for the fact that the selection of points included in the linear fit was somewhat subjective and could affect the determination of the intersection of the two lines. Finally, we include the uncertainty of l given the fact that we have a nontrivial beam width of approximately 7°.

With these maximum velocities in mind, we were able to use Equation 2 and the clever geometry [2] from Figure 1 to determine a rotation curve for the galaxy, which is shown in Figure 5.

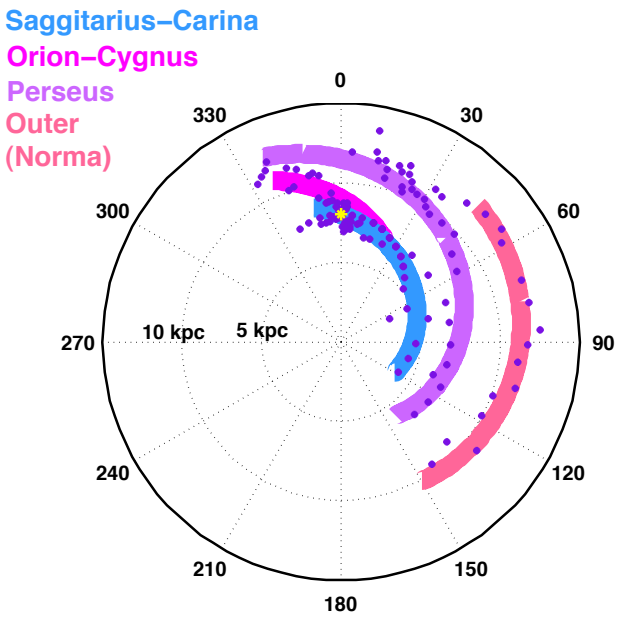

FIG. 6. We mapped the local maxima in our power spectra using Equation 5 and Equation 6. We find that the galaxy has spiral arm structure and fit the data to logarithmic spirals. The yellow star indicates the location of our solar system. The inner streak is consistent with the known intersection of the Orion-Cygnus and Saggitarius-Carina spiral arms. The middle streak is the Perseus spiral arm and the outermost streak is the outer arm that forms a continuation of the Norma arm.

IV.3. Oort's Constants

We used the local properties of the rotation curve to determine Oort's constants [6]. We fit a liner regression to data points at radii of 7 kpc and greater and used the slope and associated statistical errors to locally determine dV/dR. We found Oort's constant A to be 9.41 $\pm$ 3.95 km s^{-1}kpc^{-1} and Oort's constant B to be -17.60 $\pm$ 3.95 km s^{-1}kpc^{-1}. For a Keplerian rotation curve, we expect A to be 21.09 and for flat rotation curve, we expect A to be 13.17. We are roughly 1σ from a flat rotation curve, but we are 3σ from a Keplerian rotation curve. Therefore, we extrapolate a flat line to nearby parts of the rotation curve.

IV.4. Mapping Milky Way Spiral Arms

Using the extrapolation of the rotation curve discussed previously, we were able to map hydrogen dense regions of the galaxy by using Equation 5 and Equation 6, as well as the knowledge of local maxima in our power spectra at galactic longitudes between 30° and 250°. We mapped out these hydrogen dense regions in Figure 6.

V. CONCLUSIONS

Our solar brightness temperature is consistent with the hypothesis that the sun is in its quiet sun phase [3], meaning that there was very little exotic solar activity at the time of taking data.

Our rotation curve is inconsistent with the Keplerian prediction based on the assumption that most of the mass of the galaxy is densely concentrated in the central bulge. We can see this both by visually looking at the rotation curve and by noting that this prediction is 3σ away from our experimentally determined value of Oort's constants. Our data is far more consistent with a flat rotation curve, which means that our galaxy has a mass profile similar to that of a singular isothermal sphere, which corresponds to a mass density that goes roughly as $1/r^2$ [7]. Ordinary luminous matter cannot account for this mass density profile, which means that there must be some form of non-luminous matter that is accounting for the extra mass.

Finally, we mapped high-density regions and found these to be consistent with the intersection of the Orion-Cygnus and Saggitarius-Carina spiral arms as well as the Perseus and Norma spiral arms [1].

Our experiment could be improved upon in the future by taking even longer integrations, by using a telescope with higher angular resolution, and by taking data in a radio-quiet environment so as not to have radio stations and cell phone towers washing out galactic structure. However, despite all these shortcomings, we can see that the data we got is consistent with previously observed phenomena.

[1] F. H. Shu, *The Physical Universe.* 1982: Mill Valley, CA, University Science Books.

[2] D. Mihalas and J. Binney, *Galactic Astronomy.* 1968: San Francisco,W.H. Freeman.

[3] John D. Kraus, *Radio Astronomy of the Sun.* 1986

[4] Junior Lab Staff, *21 cm Radio Astrophysics.* 2012: http://web.mit.edu/8.13/www/JLExperiments/JLExp46.pdf

[5] H.C. Van de Hulst, *The Spiral Structure of the Outer Part of the Galactic System Derived from the Hydrogen Emission at 21cm Wave Length.* 1954: Bulletin of the Astronomical Institutes of the Netherlands, Vol. 12, Number 452

[6] J. H. Oort, *Observational evidence confirming Lindblad's hypothesis of a rotation of the galactic system.* 1927: Bulletin of the Astronomical Institutes of the Netherlands

[7] J. Binney and S. Tremaine, *Galactic Dynamics.* 1987: Princeton University Press

[8] Clemens et al., *The Galactic Disk Rotation Curve.* 1985: Astrophysical Journal, Vol. 295

ACKNOWLEDGMENTS

All fits were made using the fitlin.m and levmar.m MATLAB scripts on the Junior Lab website.

K. Schutz acknowledges the Junior Lab staff for their helpful commentary. She also wishes to thank Edward Mazenc, Emily Nardoni, and Adrian Liu for their continued support and encouragement.